Geophysical Research Letters

RESEARCH LETTER
10.1029/2018GL077853

A TKE-Based Framework for Studying Disturbed Atmospheric Surface Layer Flows and Application to Vertical Velocity Variance Over Canopies

Marcelo Chamecki[1], **Nelson L. Dias**[2,3], **and Livia S. Freire**[3]

[1]Department of Atmospheric and Oceanic Sciences, University of California, Los Angeles, CA, USA, [2]Department of Environmental Engineering, Federal University of Paraná, Curitiba, Brazil, [3]Graduate Program in Environmental Engineering (PPGEA), Federal University of Paraná, Curitiba, Brazil

Key Points:
- The reduced TKE phase space is introduced as a tool to characterize disturbed surface layer flows
- Analysis highlights some key differences between surface layer and canopy roughness sublayer flows
- Vertical velocity variance over canopies is strongly linked to the imbalance between local production and dissipation of TKE

Supporting Information:
- Supporting Information S1

Correspondence to:
M. Chamecki,
chamecki@ucla.edu

Citation:
Chamecki, M., Dias, N. L., & Freire, L. S. (2018). A TKE-based framework for studying disturbed atmospheric surface layer flows and application to vertical velocity variance over canopies. *Geophysical Research Letters*, *45*, 6734–6740. https://doi.org/10.1029/2018GL077853

Received 8 MAR 2018
Accepted 9 JUN 2018
Accepted article online 19 JUN 2018
Published online 7 JUL 2018

Abstract We propose an approach to study disturbed surface layer flows based on a simplified form of the turbulent kinetic energy (TKE) budget equation (the *reduced TKE budget*), which can be represented by a two-dimensional phase space. The phase space provides a way to quantify relative contributions of shear and buoyancy production/destruction of TKE, as well as the local imbalance between local production and dissipation. In this framework, Monin-Obukhov Similarity Theory represents one possible approach to reduce the dimensionality of the phase space. We apply this framework to study the vertical velocity variance in the canonical surface layer and in the canopy roughness sublayer above the Amazon forest. Results reveal interesting insight into the behavior of the vertical velocity variance over forests, linking its magnitude to the imbalance between local production and dissipation of TKE.

Plain Language Summary The whirling wind motions in the lowest 100 m of the atmosphere play an important role in transporting energy, gases, and particles away from and toward the land surface. These exchanges comprise an important part of the atmosphere-biosphere interaction. Quantifying and predicting the energy available to promote this mixing is critical to better understand the level of interactions between the atmosphere and the biosphere. However, the predictors of energy content are strongly linked to the surface properties, and theories that work over grass fields do not work over forests or urban areas. Thus far, each surface type has been studied separately and some are better understood than others. In this paper we propose the first step toward a more unified description of the energy available to promote vertical mixing valid across different surface types. We use observational data collected over a grass field and over the Amazon rainforest to illustrate the use of this new framework. Further studies will be required to understand its full capabilities and limitations.

1. Introduction

The Monin-Obukhov Similarity Theory (MOST) developed by Obukhov (1946) and Monin and Obukhov (1954) set out the basic framework to approach the constant flux atmospheric surface layer (ASL). The observational work that followed culminated in the Kansas and Minnesota field experiments (Kaimal & Wyngaard, 1990), which provided ample support for MOST and a wealth of data allowing for refinements and extensions of the theory (e.g., Businger et al., 1971; Kaimal, 1973; Kaimal et al., 1972; Wyngaard & Coté, 1971; Wyngaard et al., 1971). The combination of the original similarity theory and the analysis of these field data elevated the ASL to a status of a *canonical flow* in turbulence textbooks. Despite the challenges that still exist, the basic features of this idealized surface layer were well understood in the mid-1970s. Many studies thereafter have focused on more complex surface layers, as those that arise in the presence of *disturbances*. Examples include flows over gentle topography or ocean waves, sloping terrain, vegetation and urban canopies, unsteady conditions, and surface heterogeneity. Hereafter, we refer to this collection of more complex flows near the ground as *disturbed surface layers* and seek a framework capable of identifying and quantifying differences between disturbed surface layers and the canonical MOST surface layer.

Recent efforts have shown that for unstratified flows, some universal scalings of turbulence structure may exist in which the ratio between local shear production and turbulent kinetic energy (TKE) dissipation plays a critical role (Davidson & Krogstad, 2014; De Silva et al., 2015; Pan & Chamecki, 2016). These efforts have also

been extended to turbulence in the canonical ASL (Chamecki et al., 2017), with the ratio between local buoyancy production and TKE dissipation appearing as an additional parameter. This modern framework seems to emphasize, perhaps once again, that the TKE budget is a critical component of any systematic study of canonical and disturbed surface layers. MOST is in many ways motivated by the TKE budget (or at least, in some ways, by the buoyancy production term). In the theory, a proper analysis of the TKE budget consists of writing it in dimensionless form with MOST scaling, and stipulating that each dimensionless term is a function of Obukhov's stability parameter (e.g., Li et al., 2008; Sjöblom & Smedman, 2002; Wyngaard & Coté, 1971).

In the present work we take a different approach and start from the TKE budget to build a new framework. In particular, we define a *reduced TKE budget*, which can be represented by a two-dimensional phase space. In this framework, MOST represents one possible approach to reduce the dimensionality of the phase space. In this sense, the proposed framework is more general and can be used to assess whether MOST (or any other reduction to a one-dimensional representation) is reasonable or not. It can also be used to study the larger class of disturbed surface layers, in which MOST is typically assumed not to hold. We introduce the approach in section 2 and present sample applications to measurements in the ASL and the canopy roughness sublayer above a forest in section 3. Before we proceed, though, it is important to bear in mind that MOST is both a predictive model and a diagnostic tool to understand ASL turbulence. Here we focus on the latter and develop a more general framework to study canonical and disturbed surface layers. At this point, the framework has no predictive capabilities.

2. The Reduced TKE Phase Space

We start from the assumption that the essential information of canonical and disturbed ASL flows is contained in the TKE budget, which is written as

$$\underbrace{-\overline{u'w'}\frac{\partial \bar{u}}{\partial z}}_{P} + \underbrace{\beta\overline{w'\theta'}}_{B} - \epsilon = \underbrace{\frac{\partial \bar{e}_k}{\partial t} + \bar{u}\frac{\partial \bar{e}_k}{\partial x} + \frac{1}{\rho}\frac{\partial \overline{u_i' p'}}{\partial x_i} + \frac{\partial \overline{u_i' e}}{\partial x_i}}_{R}, \tag{1}$$

where $e = (1/2)u_i'u_i'$ (with implicit summation over repeated indices) and conventional notation in ASL turbulence is used. The only assumption invoked here is that the mean flow is given by $\bar{u}(z)$, which includes the assumption that $\bar{v} = \bar{w} = 0$. The terms on the left-hand side represent local shear production (P), buoyancy production/destruction (B), and TKE dissipation rate (ϵ), with all the terms that could produce a local imbalance between production and dissipation lumped together into the residual term (R) on the right-hand side. It is typical to make the TKE budget dimensionless using the friction velocity (u_*) and the distance to the ground (z) as the relevant velocity and length scales, leading to the usual dimensionless form used in MOST (Kaimal & Finnigan, 1994). Instead, we adopt the local TKE dissipation rate as a scaling parameter and write

$$\frac{P}{\epsilon} + \frac{B}{\epsilon} - 1 = \frac{R}{\epsilon}. \tag{2}$$

We refer to this form of the TKE budget, in which one cannot distinguish the causes of local imbalance, as the reduced TKE budget. Equation (2) shows that the reduced TKE budget can be described by two dimensionless parameters, which we choose to be P/ϵ and B/ϵ. Thus, the reduced TKE budget given by equation (2) can be fully characterized in the two-dimensional phase space depicted in Figure 1. Some features of the phase space are discussed below.

The black solid slanted line in Figure 1 represents states of local balance between production and dissipation of TKE (i.e., $R = 0$), with points to the right (yellow region) and left (red region) representing $(P + B) > \epsilon$ and $(P+B) < \epsilon$, respectively. Lines parallel to the local balance line are isolines of R/ϵ, so that the local imbalance for any point on the diagram is proportional to its distance to the local balance line (actually, $R/\epsilon = \sqrt{2}d$, d being the distance between the point and the local balance line). We point out that the definition of local imbalance employed here is the same as in Sjöblom and Smedman (2002), representing several physical processes that break the balance between local production and local dissipation of TKE. This is different from the most usual definition used in previous studies in which the imbalance is defined as the remainder of a simplified version of the TKE budget (Li et al., 2008; Wyngaard & Coté, 1971).

Atmospheric stability is represented in the phase space by the flux Richardson number $\mathrm{Ri_f} = -B/P$. Lines of constant $\mathrm{Ri_f}$ are shown with dashed lines. Linking the phase space to MOST is possible in the constant

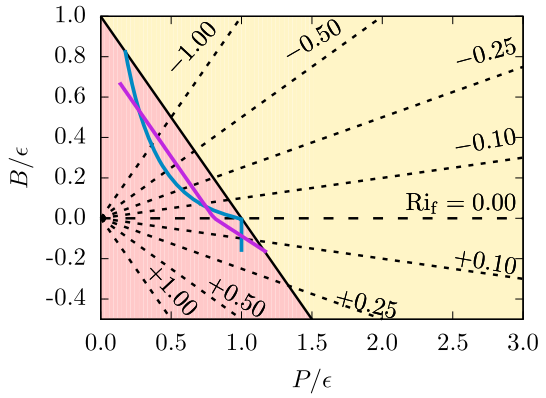

Figure 1. Two-dimensional phase space associated with the reduced turbulent kinetic energy budget given by equation (2). Lines indicate states of local balance between production and dissipation (black solid line), lines of constant flux Richardson number (dashed lines), and trajectories corresponding to Monin-Obukhov Similarity Theory based on the empirical functions from Kansas (Kaimal & Finnigan, 1994; blue line) and those proposed by Högström (1988, 1990; purple line).

flux layer. In this case, we have $\mathrm{Ri_f} = (z/L)\phi_m^{-1}$, where L is the Obukhov length scale. As noted by Chamecki et al. (2017), $P/\epsilon = \phi_m/\phi_\epsilon$ and $B/\epsilon = (-z/L)/\phi_\epsilon$, where $\phi_m(z/L)$ and $\phi_\epsilon(z/L)$ are the similarity functions for the mean shear and the dissipation rate of TKE, respectively. Thus, a trajectory representing the variation in the MOST parameter z/L can be determined from the similarity functions for shear and dissipation rate. Trajectories obtained from the empirical similarity functions from the Kansas experiment (see Kaimal & Finnigan, 1994; in blue) and those proposed by Högström (1988, 1990; in purple) are illustrated in the phase space for the range $z/L = -2$ (upper left end of lines) and $z/L = 1$ (lower right end).

An important question that presents itself at this point is associated with the possibility of reduction in dimensionality: under which conditions can the two-dimensional phase space be further reduced into a one-dimensional space represented, as an example, by $\mathrm{Ri_f}$ or z/L? Obviously, the trivial case is the one for which there exists an explicit relationship between the two independent variables P/ϵ and B/ϵ, such as imposed by the reduced TKE budget by restricting the residual R/ϵ to be either a constant or a function of, say, P/ϵ. We use two data sets to illustrate how this question can be addressed in the next section.

Before we proceed, a few notes are due. First, the framework presented above is not based on a choice of appropriate scales followed by dimensional analysis. Instead, it is completely based on the ability of the reduced TKE budget in describing the characteristics of the turbulent flow. A direct implication is that all the variables involved are local, in the spirit of the local similarity of Nieuwstadt (1984). Thus, they are not explicitly tied to the boundary conditions as is the case of MOST. We trade the predictive capabilities of MOST for an enhanced ability of the proposed framework to study disturbed ASL flows. In this sense, we also note that each state of the ASL is represented by one point on the phase space, and a sequence of points can be used to represent the time evolution of turbulence (e.g., a diurnal cycle) or changes along a direction of flow inhomogeneity.

3. Application to Field Data

To illustrate the use of the reduced TKE phase space, we contrasted the behavior of the vertical velocity variance in the canonical surface layer with that in the canopy roughness sublayer above the Amazon forest. For this purpose, we employed the AHATS (Salesky & Chamecki, 2012; University Corporation for Atmospheric Research-National Center for Atmospheric Research — Earth Observing Laboratory, 1990) and the GoAmazon (Freire et al., 2017; Fuentes et al., 2016) data sets. The two experiments have been described in detail in the literature, and here we include only key information. The AHATS profile tower consisted of six sonic anemometers at heights of $z = 1.51$, 3.30, 4.24, 5.53, 7.08, and 8.05 m. We used data from the period between 25 June and 17 July and calculated statistics for runs of 36.4 min. Runs satisfying three criteria were selected for further analysis: azimuth wind direction within ±45° (in the frame of reference of the sonic anemometer), stationarity of the horizontal wind (Vickers & Mahrt, 1997), and the existence of an inertial subrange in the second-order structure function with slope within 10% of the theoretical prediction of 2/3 (Kolmogorov, 1941). In addition, to eliminate a few outliers and facilitate bin averaging, we removed the few points with local stability parameter $|(z - d_0)/\Lambda| > 5$. For the GoAmazon experiment, we used the uppermost three sonic anemometers at heights $z = 34.9$, 40.4, and 48.2 m, corresponding to normalized heights z/h =1.00, 1.15, and 1.38 (h being the approximate canopy top). We used data from the entire field campaign, extending from March 2014 to January 2015. Statistics were calculated for 30-min runs, and the same selection criteria were applied, except that we extended the azimuth wind direction limit to ±90° (this increased the number of runs available without significant changes in the trends observed). In addition, we also eliminated the few runs with negative shear production or very small TKE dissipation rates (with ad hoc limit set to $\epsilon < 5 \times 10^{-5}$ m^2/s^3). These selection criteria resulted in a total of 1,154 samples for the AHATS and 2,061 samples for the GoAmazon experiment. Mean velocity gradients needed to estimate the shear production were determined using a second-order polinomial fit in ln(z) (Högström, 1988), and the TKE dissipation rates were estimated from inertial subrange scaling for the second-order longitudinal structure function following Chamecki and Dias (2004).

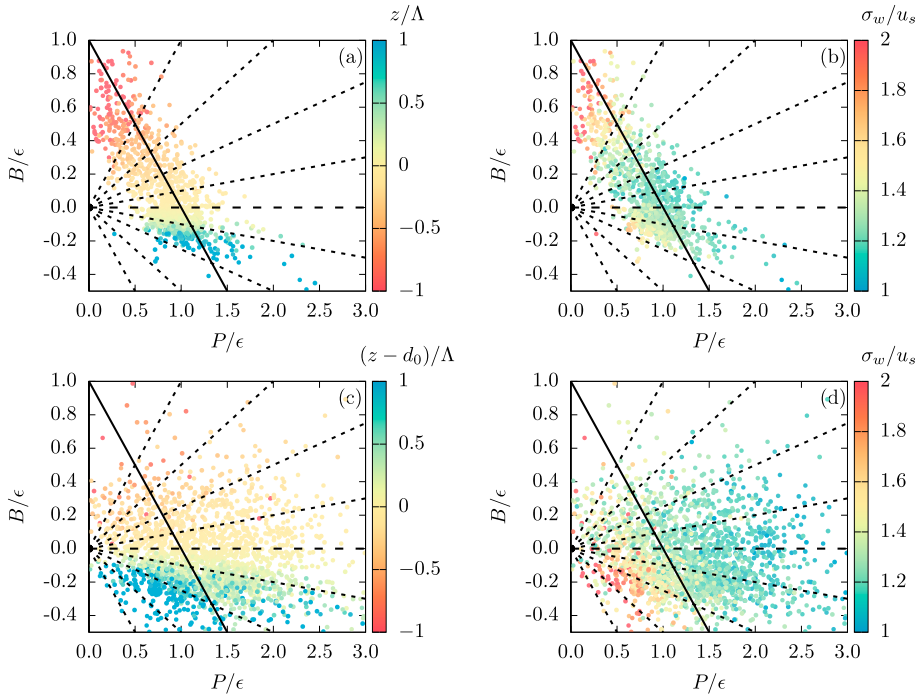

Figure 2. Field data displayed on the turbulent kinetic energy phase space for the canonical surface layer (AHATS, a and b) and the canopy roughness sublayer (GoAmazon, c and d) color coded based on value of local stability parameter (a, c) and σ_w/u_s (b, d). All measurement heights are displayed together.

Despite the inertial subrange slope observed in the longitudinal structure function, both data sets present large deviations from local isotropy at the scales sampled by the sonic anemometers as previously reported by Chamecki and Dias (2004) and Babić and Rotach (2018). This issue is discussed in more detail in the supporting information. For the GoAmazon data, when calculating the MOST stability parameter, heights are reported as distance from the displacement height (d_0) estimated from the inside canopy measurements of momentum flux (Jackson, 1981; Pan et al., 2016). Finally, we note that all quantities used here were calculated at the height of the measurements (e.g., we used local momentum and buoyancy fluxes and not their surface counterparts). To make this clear, we denote the local friction velocity by u_s and the local Obukhov length scale by Λ. More details of the data processing are presented in the supporting information.

3.1. Canonical Surface Layer

Data from the AHATS field campaign are displayed in the reduced TKE phase space in Figure 2a color coded by the value of the local similarity parameter z/Λ (note that for the canonical surface layer $z/\Lambda \approx z/L$, though). In this figure, each point corresponds to one 36.4-min run, and data from all heights are displayed together since all the trends are independent of height. AHATS data fall mostly parallel to the local balance line with limited spread, implying that local imbalance is more or less constant (and on average very close to zero). The high degree of organization in the colors reflects an expected relationship between z/Λ and $\mathrm{Ri_f}$. Unstable runs are more spread out along the balance line than the stable ones, which stems from the fact that the range $-2 \leq z/\Lambda \leq 0$ maps into a wider range of $\mathrm{Ri_f}$ than its stable counterpart. Note that very few points exist for $\mathrm{Ri_f} > 0.25$, considered a limit to the applicability of MOST (Grachev et al., 2013).

To illustrate one use of the reduced phase space, we choose to investigate the behavior of the vertical velocity variance. This choice is motivated in part by the relative success of scaling this variable using MOST, and in part by the important role the vertical velocity variance plays in vertical mixing in the surface layer. The same data from Figure 2a are shown in Figure 2b, now color coded by values of σ_w/u_s. The organization of color patterns is suggestive that the vertical velocity variance can be well characterized in terms of the two variables in the reduced TKE budget, lending support to the framework proposed here. A visual comparison between the patterns displayed in Figures 2a and 2b suggests that most variability in σ_w/u_s is in the direction parallel to the variability in z/Λ. In other words, if we consider a subspace of $(P/\epsilon, B/\epsilon)$ defined by z/Λ, the projection

of the function $[\sigma_w/u_s](P/\epsilon, B/\epsilon)$ onto the subspace captures most of the signal. Thus, most of the variability in σ_w/u_s can be represented by a functional relationship with z/Λ and the reduction in dimensionality represented by MOST is appropriate.

3.2. Canopy Roughness Sublayer

Data for the roughness sublayer above the Amazon forest are displayed in the same way as for the AHATS in Figures 2c and 2d. Perhaps the first difference to be noted is that the canopy data span a much wider range of deviations of local balance (as measured by R/ϵ), occupying a much larger portion of the phase space. Consistent with current understanding of near-neutral canopy flows (Finnigan, 2000), we typically observe $(P+B) > \epsilon$ at $z/h = 1.00$ and a tendency for points to move closer to the balance line with increasing distance from the canopy top (see figure in supporting information). The relation between $(z-d_0)/\Lambda$ and $\mathrm{Ri_f}$ observed in Figure 2c is very similar to the surface layer one, perhaps suggesting the existence of some universality (this is not a trivial result, given that the mean velocity gradient enters in the definition of $\mathrm{Ri_f}$ but not in $(z-d_0)/\Lambda$). We also point out that the Amazon data display a large number of runs with $(P+B) < \epsilon$ (the region below the black line in Figure 2c), including many below the empirical limit of $\mathrm{Ri_f} > 0.25$. This is an interesting feature that may deserve future attention.

Similarly to the AHATS data, there is remarkable organization in σ_w/u_s when plotted on the phase space (Figure 2d). Data from different measurement heights collapse well, lending support to the assumption that the reduced TKE phase space provides a reasonably complete description of σ_w/u_s. Visual comparison between Figures 2b and 2d suggests a very different conclusion from AHATS with respect to the reduction of dimensionality. The vertical velocity variance displays significant variation for a fixed $\mathrm{Ri_f}$, while $(z-d_0)/\Lambda$ is approximately constant. Thus, a significant portion of the variability in σ_w/u_s cannot be captured by an atmospheric stability parameter (be that $\mathrm{Ri_f}$ or $(z-d_0)/\Lambda$). In reality, most of the variability in σ_w/u_s can be represented by P/ϵ, suggesting that shear production is the dominant mechanism in the GoAmazon data set. An even clearer relationship exists between σ_w/u_s and the local TKE imbalance R/ϵ. Thus, if one seeks a reduction in dimensionality to describe $[\sigma_w/u_s](P/\epsilon, B/\epsilon)$, the best options would be either $[\sigma_w/u_s](P/\epsilon)$ or $[\sigma_w/u_s](R/\epsilon)$.

A comparison between two reductions in dimensionality, one based on stability $[\sigma_w/u_s]((z-d_0)/\Lambda)$ and the other based on TKE imbalance $[\sigma_w/u_s](R/\epsilon)$, is shown in Figure 3 for both data sets. While there is a clear advantage in the adoption of MOST for the canonical surface layer, for the GoAmazon the use of R/ϵ as a variable to describe the variability in σ_w/u_s is more appropriate. This can be inferred by the reduced scatter in Figure 3d when compared to Figure 3c, as well as by the better collapse of data from different heights.

Before proceeding, a note regarding the issue of self-correlation is in order. This concern arises when σ_w/u_s is displayed against P/ϵ, as in Figures 2b and 2d, or when it is displayed as a function of $R/\epsilon = P/\epsilon + B/\epsilon - 1$ as in Figures 3b and 3d. In these cases, because shear production is given by $P = u_s^2(\mathrm{d}\bar{u}/\mathrm{d}z)$, there is the potential for self-correlation due to the presence of u_s in both dimensionless variables. An in-depth analysis of self-correlation based on the randomization approach (Klipp & Mahrt, 2004) is presented in the supporting information. The randomization approach suggests that self-correlation is not the main driver of the trends reported here and its effects seem to be, at most, very small.

Interestingly, and maybe counterintuitively, positive imbalance (i.e., local production larger than local dissipation) is associated with lower values of σ_w/u_s (Figure 3d). While an in-depth analysis of the causes for this behavior is beyond the scope of this paper, we can understand this behavior if we consider only shear production (which is the dominant mechanism of TKE production for this data set). The shear production P is a source of TKE that impacts directly the streamwise variance σ_u^2. This energy is redistributed to the vertical (and lateral) variance by the pressure isotropization term. We envision the total shear production being split into two components: one cascading to smaller scales and the other being transported by turbulence to other regions (e.g., into the canopy). In this sense, a larger imbalance means that from the total production, a larger fraction is transported elsewhere and a smaller fraction is available to be redistributed to σ_w by pressure isotropization. While this is not the only possible explaining mechanism, it is one explanation for the observed behavior.

Before concluding, we make one last observation regarding the observed patterns in $[\sigma_w/u_s](P/\epsilon, B/\epsilon)$. Figures 2b and 2d share many similarities. However, there is not much overlap in the regions of the phase space occupied by the two data sets. It is conceivable that the surface $[\sigma_w/u_s](P/\epsilon, B/\epsilon)$ could be the same for both data sets, suggesting some degree of universality between the two flows. If this were true,

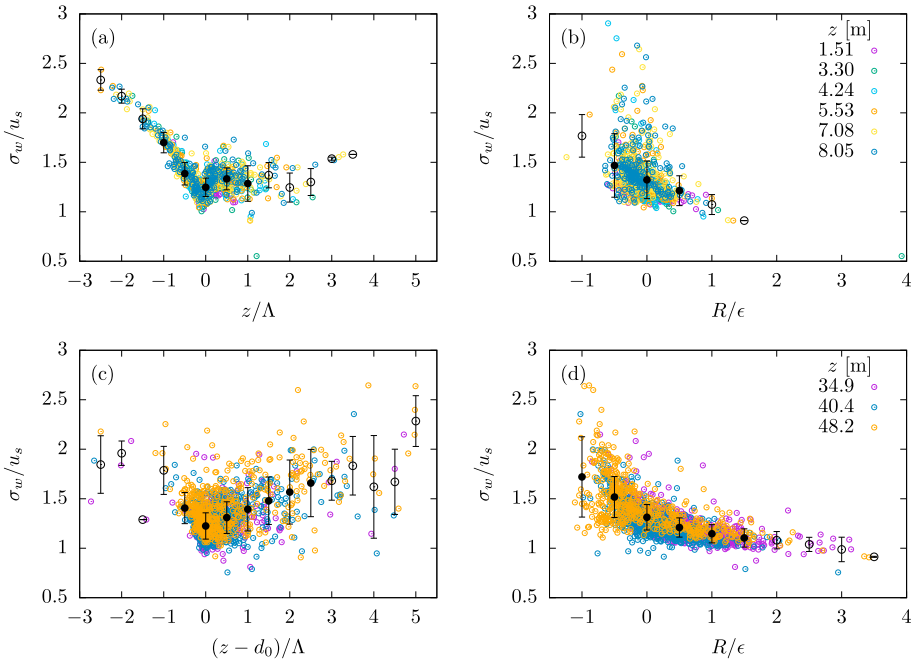

Figure 3. Normalized root mean square of vertical velocity from surface layer (a, b) and canopy roughness sublayer (c, d) displayed as a function of stability parameter (a, c) and local imbalance R/ϵ (b, d). Solid/open circles indicate bin-averaged values for bins with more/less than 25 samples (error bars represent one standard deviation).

the different behaviors of σ_w/u_s in the canonical surface layer and in the canopy roughness sublayer would have to emerge from the fact that the two flows occupy different regions of the phase space. More studies are clearly necessary to elucidate this matter.

4. Conclusion

We have proposed a new framework to study perturbed surface layer flows based on a reduced form of the TKE budget. The framework consists of displaying data on a two-dimensional phase space that completely characterizes the reduced budget and includes information of the relative contributions of the two production mechanisms (shear and buoyancy), as well as the local imbalance between production and dissipation. When this framework is applied to the canonical surface layer, MOST emerges as an obvious approach to reduce the dimensionality via parametric representation. For the canopy roughness sublayer, however, this is clearly not the case. Nevertheless, the framework suggests that a possible reduction in dimensionality for the roughness sublayer can be achieved in terms of the imbalance between local production and dissipation of TKE normalized by the dissipation rate.

It is perhaps premature to claim that the proposed phase space representation is indeed a useful tool in studying the *overall* class of perturbed surface layers. After all, statistically steady flow above canopies may very well be the simplest of the disturbed surface layers, as it still has only one direction of nonhomogeneity. Application of this framework to other disturbed surface layers will be needed to test the limits of applicability of this technique.

Acknowledgments
The AHATS data were collected by NCAR's Integrated Surface Flux Facility. We would like to acknowledge operational, technical, and scientific support provided by NCAR's Earth Observing Laboratory, sponsored by the National Science Foundation. The GoAmazon 2014/5 field study was supported by the U.S. Department of Energy (grant SC0011075) and benefited from logistic support provided by the Large-scale Biosphere-Atmosphere Experiment in Amazonia (LBA). M. C. acknowledges partial funding from the U.S. Department of Energy (grant SC0011075). The processed data needed for reproducing the figures are available from the authors upon request (chamecki@ucla.edu).

References

Babić, K., & Rotach, M. (2018). Turbulence kinetic energy budget in the stable boundary layer over a heterogeneous surface. https://doi.org/10.1002/qj.3274

Businger, J. A., Wyngaard, J. C., Izumi, Y., & Bradley, E. F. (1971). Flux-profile relationships in the atmospheric surface layer. *Journal of the Atmospheric Sciences*, *28*(2), 181–189.

Chamecki, M., & Dias, N. (2004). The local isotropy hypothesis and the turbulent kinetic energy dissipation rate in the atmospheric surface layer. *Quarterly Journal of the Royal Meteorological Society*, *130*(603), 2733–2752.

Chamecki, M., Dias, N. L., Salesky, S. T., & Pan, Y. (2017). Scaling laws for the longitudinal structure function in the atmospheric surface layer. *Journal of the Atmospheric Sciences*, *74*(4), 1127–1147.

Davidson, P., & Krogstad, P.-Å. (2014). A universal scaling for low-order structure functions in the log-law region of smooth-and rough-wall boundary layers. *Journal of Fluid Mechanics*, *752*, 140–156.

De Silva, C., Marusic, I., Woodcock, J., & Meneveau, C. (2015). Scaling of second-and higher-order structure functions in turbulent boundary layers. *Journal of Fluid Mechanics*, *769*, 654–686.
Finnigan, J. (2000). Turbulence in plant canopies. *Annual Review of Fluid Mechanics*, *32*(1), 519–571.
Freire, L., Gerken, T., Ruiz-Plancarte, J., Wei, D., Fuentes, J., Katul, G., et al. (2017). Turbulent mixing and removal of ozone within an Amazon rainforest canopy. *Journal of Geophysical Research*, *122*, 2791–2811. https://doi.org/10.1002/2016JD026009
Fuentes, J. D., Chamecki, M., Nascimento dos Santos, R. M., Von Randow, C., Stoy, P. C., Katul, G., et al. (2016). Linking meteorology, turbulence, and air chemistry in the Amazon rain forest. *Bulletin of the American Meteorological Society*, *97*(12), 2329–2342.
Grachev, A. A., Andreas, E. L., Fairall, C. W., Guest, P. S., & Persson, P. O. G. (2013). The critical richardson number and limits of applicability of local similarity theory in the stable boundary layer. *Boundary-Layer Meteorology*, *147*(1), 51–82.
Högström, U. (1988). Non-dimensional wind and temperature profiles in the atmospheric surface layer: A re-evaluation. *Boundary-Layer Meteorology*, *42*(1), 55–78.
Högström, U. (1990). Analysis of turbulence structure in the surface layer with a modified similarity formulation for near neutral conditions. *Journal of the Atmospheric Sciences*, *47*(16), 1949–1972.
Jackson, P. (1981). On the displacement height in the logarithmic velocity profile. *Journal of Fluid Mechanics*, *111*, 15–25.
Kaimal, J. (1973). Turbulenece spectra, length scales and structure parameters in the stable surface layer. *Boundary-Layer Meteorology*, *4*(1-4), 289–309.
Kaimal, J. C., & Finnigan, J. J. (1994). *Atmospheric boundary layer flows: Their structure and measurement*. New York: Oxford University Press.
Kaimal, J., & Wyngaard, J. (1990). The Kansas and Minnesota experiments. *Boundary-Layer Meteorology*, *50*(1), 31–47.
Kaimal, J. C., Wyngaard, J., Izumi, Y., & Coté, O. (1972). Spectral characteristics of surface-layer turbulence. *Quarterly Journal of the Royal Meteorological Society*, *98*(417), 563–589.
Klipp, C. L., & Mahrt, L. (2004). Flux–gradient relationship, self-correlation and intermittency in the stable boundary layer. *Quarterly Journal of the Royal Meteorological Society*, *130*(601), 2087–2103.
Kolmogorov, A. N. (1941). The local structure of turbulence in incompressible viscous fluid for very large Reynolds numbers. *Dokl Akad Nauk SSSR*, 30, 299–303.
Li, X., Zimmerman, N., & Princevac, M. (2008). Local imbalance of turbulent kinetic energy in the surface layer. *Boundary-Layer Meteorology*, *129*(1), 115–136.
Monin, A., & Obukhov, A. (1954). Basic laws of turbulent mixing in the surface layer of the atmosphere. *Trudy Akademiya Nauk SSSR Geofizicheskogo Instituta*, *151*, 163–187.
Nieuwstadt, F. T. (1984). The turbulent structure of the stable, nocturnal boundary layer. *Journal of the Atmospheric Sciences*, *41*(14), 2202–2216.
Obukhov, A. (1946). Turbulentnost'v temperaturnoj-neodnorodnoj atmosfere (Turbulence in an atmosphere with a non-uniform temperature). *Trudy Inst Theor Geofiz AN SSSR*, *1*, 95–115. (translation in: Boundary-Layer Meteorol. 1971, 2: 7-29).
Pan, Y., & Chamecki, M. (2016). A scaling law for the shear-production range of second-order structure functions. *Journal of Fluid Mechanics*, *801*, 459–474.
Pan, Y., Chamecki, M., & Nepf, H. M. (2016). Estimating the instantaneous drag–wind relationship for a horizontally homogeneous canopy. *Boundary-Layer Meteorology*, *160*(1), 63–82.
Salesky, S. T., & Chamecki, M. (2012). Random errors in turbulence measurements in the atmospheric surface layer: Implications for monin–obukhov similarity theory. *Journal of the Atmospheric Sciences*, *69*(12), 3700–3714.
Sjöblom, A., & Smedman, A.-S. (2002). The turbulent kinetic energy budget in the marine atmospheric surface layer. *Journal of Geophysical Research*, *107*(C10), 3142.
University Corporation for Atmospheric Research-National Center for Atmospheric Research — Earth Observing Laboratory (1990). NCAR integrated surface flux system (ISFS). https://doi.org/10.5065/D6ZC80XJ
Vickers, D., & Mahrt, L. (1997). Quality control and flux sampling problems for tower and aircraft data. *Journal of Atmospheric and Oceanic Technology*, *14*(3), 512–526.
Wyngaard, J., & Coté, O. (1971). The budgets of turbulent kinetic energy and temperature variance in the atmospheric surface layer. *Journal of the Atmospheric Sciences*, *28*(2), 190–201.
Wyngaard, J., Izumi, Y., & Collins, S. A. (1971). Behavior of the refractive-index-structure parameter near the ground. *Journal of the Optical Society of America*, *61*(12), 1646–1650.